Farzan, Afsoon; Borandeh, Sedigheh; Seppälä, Jukka

Conductive polyurethane/PEGylated graphene oxide composite for 3D-printed nerve guidance conduits

Published in:
European Polymer Journal

DOI:
10.1016/j.eurpolymj.2022.111068

Published: 15/03/2022

Document Version
Publisher's PDF, also known as Version of record

European Polymer Journal 167 (2022) 111068

Contents lists available at ScienceDirect

European Polymer Journal

journal homepage: www.elsevier.com/locate/europolj

Conductive polyurethane/PEGylated graphene oxide composite for 3D-printed nerve guidance conduits

Afsoon Farzan [1], Sedigheh Borandeh [1], Jukka Seppälä [*]

Polymer Technology, School of Chemical Engineering, Aalto University, Kemistintie 1, 02150 Espoo, Finland

ARTICLE INFO

Keywords:
3D printing
Solvent-free polyurethane
Graphene oxide
Nerve regeneration
Stereolithography

ABSTRACT

Conductive polymeric nanocomposites have made significant contributions in nerve regeneration. To this aim, the best results are obtained by using nerve guidance conduits (NGCs) with conductive, bio-compatible, biodegradable tubes as well as special topographical features. In this study, biodegradable, conductive, solvent-free polyurethane/PEGylated graphene oxide (PU/PEG-GO) composites were synthesized and successfully 3D printed into flexible nerve conduits with different precise geometries, such as hollow, porous, and grooved tubes, using stereolithography. The composite containing 5% PEG-GO showed the highest tensile stress (3.51 ± 0.54 MPa), tensile strain at break (~170%), and conductivity (1.1×10^{-3} S/cm) with the lowest contact angle of 72° attributing to the strong interfacial interactions between PEG-GO nanosheets and the PU matrix. Moreover, the PU/PEG-GO 5% exhibited higher compression strength compared with pure PU and showed appropriate enzymatic degradation after 6 weeks, which is expected to last sufficiently for an efficient nerve regeneration. Altogether the 3D-printed, conductive, biodegradable, and flexible PU/PEG-GO 5% conduit with precise geometry has potential as NGCs for peripheral nerve regeneration.

1. Introduction

The repair of peripheral nerve injuries is one of the most critical and challenging clinical procedures with more than 100,000 cases in Europe and the United States annually [1]. Peripheral nerve injuries can occur due to accident, congenital defects, and cancer [2]. Generally, two main methods are employed to repair damaged nerves, including implantation of autografts/allografts and incorporation of artificial nerve guidance conduits (NGCs) in the damaged site of the peripheral nerve [3–5]. However, there are limitations in using autografts/allografts, such as morbidity of the donor site, mismatching of the size, and limited accessibility, which lead to the introduction and development of alternatives, such as NGCs [6]. As such, a broad range of natural and synthetic materials have been investigated for the fabrication of NGCs, including among others, silk, collagen, chitosan, polyurethanes (PUs), and polycaprolactones (PCL) [7]. Among all synthetic materials, PUs have received special attention regarding the fabrication of NGCs because of their tunable structure and good mechanical properties [8]. PUs are block copolymers, which consist of soft segments and hard segments [9]. For PU elastomers, optimization of toughness, elasticity, biocompatibility, and biodegradability is possible by adjustment of the soft and hard segment ratios [8]. The PU nerve conduit based on PCL and polyethylene glycol (PEG) has been used to develop NGCs for peripheral nerve regeneration [10–13]; however, they have been produced with various manufacturing methods.

There are different methods for fabrication of NGCs, such as injection molding, film rolling, extrusion, dip coating, and rapid prototyping (RP) technique [7]. RP is an emerging manufacturing method, which is highly effective for producing complicated and precise 3D structures with complex geometry [14]. One of the fast growing 3D-printing techniques in biomedical engineering is stereolithography (SLA), which is distinguished by its superior speed and high resolution for manufacturing complex and specific structures [15]. To improve the performance of NGCs in the nerve regeneration process, applying NGCs with geometrical features, such as micron scale grooves, multi-internal channels, and fibers, have been investigated widely [16]. According to the literature, the morphology patterns of the NGCs are an important feature for the alignment of supporting cells and neurons; tubes with V- and slope-shaped grooves showed excellent cell elongation [17]. Furthermore, in order to stimulate, direct, and accelerate axonal

* Corresponding author.
E-mail address: jukka.seppala@aalto.fi (J. Seppälä).
[1] These authors had the same contribution.

https://doi.org/10.1016/j.eurpolymj.2022.111068
Received 7 January 2022; Received in revised form 9 February 2022; Accepted 11 February 2022
Available online 15 February 2022

elongation for the purpose of peripheral nerve regeneration, the use of conductive nerve conduits has a significant impact [18]. The electrical conductivity of the NGCs can stimulate the differentiation of mesenchymal stem cells into Schwann cells (SCs) and as a result facilitate peripheral nerve regeneration [19].

Recently, different types of conducting polymers for tissue engineering have been investigated, such as polypyrrole (PPy), polyaniline (PANI), polythiophene (PTh), poly(3,4-ethylenedioxythiophene) (PEDT, PEDOT), and their derivatives and composites [20,21]. In addition, conductive nanocomposites, such as carbon nanotubes (CNT) [22] and graphene-based nanocomposites (GNCs) [23] have been widely reported for their use in tissue engineering applications. Among all these conductive materials, GNCs have shown excellent conductivity and mechanical strength, which have significant impacts on stimulation, proliferation, and differentiation of neural stem cells [23]. However, there is a significant concern with the utilization of GNCs in biomedical applications due to the toxicity of graphene [24,25]. Functionalization of graphene has been investigated to resolve its biocompatibility concern. Surface modification with polyethylene glycol (PEG) [26] has been studied as an effective method to improve the solubility, stability, and biocompatibility of the graphene [27].

In this study, a conductive polymeric composite was prepared using PEGylated GO and PU resin and was used for the fabrication of an NGC with a 3D-printing technique. Printed tubes had precise geometrical features, which is essential for cell elongation in a suitable direction. PEGylation of GO improved homogeneity and compatibility of GO in the polymer matrix, leading to increase the conductivity and mechanical properties of composites in a suitable range for nerve regeneration. The effect of PEG-GO ratio was investigated in terms of the conductivity, thermal and mechanical properties, and wettability of the composite to find an optimal ratio for printing nerve conduits and enzymatic degradation study.

2. Experimental

2.1. Materials

Polyethylene glycol (PEG, Mn 400 g mol^{-1}), hexamethylene diisocyanate (HDI, 98%), polycaprolactone diol (PCL, Mn 530 g mol^{-1}), dibutyltin dilaurate (DBTDL, 95%), propylene carbonate, hydroxyethyl methacrylate (HEMA), sulfuric acid (H_2SO_4 98%), hydrogen peroxide (H_2O_2), graphite powder (<20 μm), potassium permanganate ($KMnO_4$), sodium metabisulfite ($Na_2O_5S_2$), potassium peroxodisulfate ($K_2O_8S_2$), and poly(ethylene glycol) methyl ether methacrylate (MPEG) were obtained from Sigma-Aldrich. Ethyl phenyl(2,4,6-trimethylbenzoyl) phosphinate (TPO) was purchased from Carbosynth. All chemicals were used as received.

2.2. Synthesis of graphene oxide (GO)

Graphene oxide (GO) was produced through the modified Hummer's synthesis method from graphite flakes [28]. Briefly, graphite powder (1 g) was poured into a cold (0 °C) mixture of concentrated H_2SO_4 (24 ml) and $NaNO_3$ (0.5 g). Then, $KMnO_4$ (3 g) was added gently. The reaction is exothermic, and the temperature should be kept below 20 °C. Then, the mixture was stirred at 35 °C for 30 min to oxidize and turn the color of the mixture from black to brownish. Afterward, the mixture was poured into 50 ml of distilled water, and the temperature was raised to 98 °C and stirred for 1 h. Finally, the reaction was terminated by adding distilled water (140 ml) and treated with H_2O_2 30% (4 ml). The sediment was collected after centrifugation for 20 min with 4000 rpm and washed twice with distilled water to eliminate impurities. Then, the product was freeze dried for 24 h.

2.3. Pegylation of GO (PEG-GO)

For the PEGylation reaction, the obtained GO (0.4 g) was dispersed in distilled water (100 ml). Then, the suspension was exfoliated by sonication at a frequency of 2.25×10^4 Hz and a power of 100 W for 15 min. Afterward, $K_2O_8S_2$ (0.1 g) and $Na_2O_5S_2$ (0.07 g) were dissolved in distilled water (2 ml) and added to the suspension as radical initiators. The mixture was stirred under purge of N_2 at 70 °C for 30 min. Then, MPEG was added dropwise, and the mixture was refluxed at 70 °C for 12 h. Finally, the product was collected after centrifugation with 12000 rpm for 1 h and washed two times with distilled water. Then, the sediment was freeze dried for 24 h.

2.4. Synthesis of polyurethane (PU) resin

A solvent-free PU resin was synthesized through a two-step polymerization as described in our previous research [29]. Briefly, polycaprolactone diol (0.01 mol), polyethylene glycol (0.01 mol), and DBTDL (catalyst) were mixed in a three-neck, round-bottom flask reactor under N_2 purge. The mixture was stirred at 60 °C for 30 min. Afterward, HDI (0.03 mol) was added dropwise to the mixture, and the reaction proceeded at 60 °C under N_2 atmosphere for 1 h. A viscous pre-polymer with active isocyanate-ended was prepared. Then, HEMA (0.02 mol) was added gently to the pre-polymer, and the reaction was mixed for a further 1 h at 60 °C. Then, the obtained viscous resin stored at room temperature in a dark place.

2.5. Preparation of composite and 3D-printed conduits

A series of composites were made using PU resin with different ratios (0.5, 1, 3, and 5% w/w) of PEG-GO in pure resin, which are subsequently abbreviated PU/PEG-GO. At first, an appropriate amount of PEG-GO was dissolved in propylene carbonate as a diluent; then, it was added to the polyurethane resin and mixed for 1 h. Finally, TPO (5% w/w of resin) was added as a photo-initiator. The ratio of resin to diluent was adjusted to be 60:40 in all composites. The prepared resin is then used for printing of different types of conduits including grooved, hollow, and porous tubes in various sizes e.g. diameter of 2–4 mm and length of 15–20 mm. After printing, propylene carbonate was removed from the printed structure using pure ethanol through solvent exchange method. Finally, ethanol was evaporated in the vacuum oven for 48 h.

2.6. Characterization

Infrared (IR) spectroscopy was employed to investigate the chemical structures of the synthesized materials, including the resin, GO, and PEG-GO, using an attenuated total reflectance (ATR–IR) Perkin Elmer spectrometer in transmission mode. The scanning number and resolution were 32 and 4 cm^{-1}, respectively.

The thermal stability of the synthesized PU/PEG-GO elastomers was measured by thermogravimetry analysis (TGA), operating a TA instrument (Q500) under N_2 atmosphere at a heating rate of 10 °C/min from 30 °C to 600 °C.

Tensile analysis was carried out utilizing cast films of PU with different ratios of PEG-GO (L = 20 mm, W = 5 mm, T = 0.2 mm) on Instron 4204 universal testing equipment. The static load cell was 100 N with a speed of 10 mm/min, and the measurement was performed at 25 °C, with a relative humidity of 50%. All samples were stored at the testing conditions (25 °C, 50% relative humidity) for 48 h prior to testing.

The compression stress–strain results were obtained using an Instron Universal testing equipment model 5944 with a 100 N load cell at 25 °C, with a relative humidity of 50%. 3D-printed samples were compressed up to approximately 80% strain with a constant rate of 1 mm/min. The compressive stress at 10%, 40%, and 80% of strain were compared for all samples.

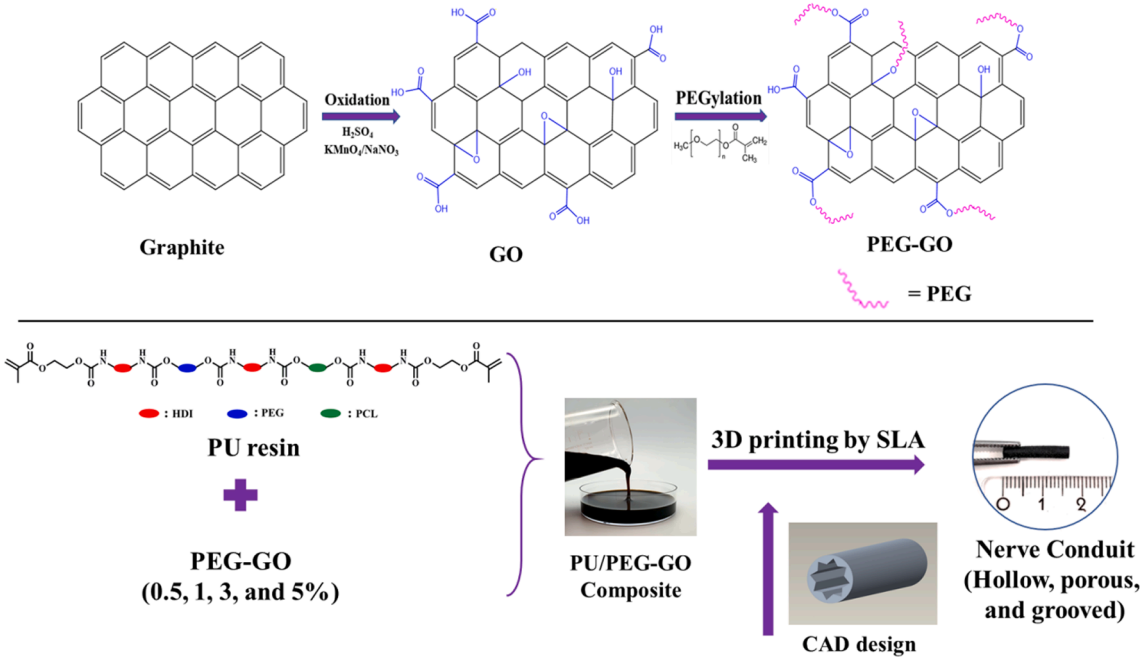

Fig. 1. Schematic procedures for synthesis of GO, PEG-GO, PU/PEG-GO composites, and 3D-printed nerve conduits.

Differential scanning calorimetry (DSC) measurements were performed with a Q2000 device (TA Instruments) to analyze all PU/PEG-GOs. The samples were heated to 200 °C at a rate of 10 °C min^{-1}, followed by cooling to −70 °C. After equilibration at −70 °C for 5 min, a second heating cycle was completed to 200 °C at a rate of 10 °C/min.

X-ray diffraction (XRD) was employed to characterize the nature of the PU films with different ratios of PEG-GO. XRD patterns were collected using a PANalytical X Pert Powder XRD (alpha-1) diffractometer with a copper target at the wavelength of λ CuKα = 1.5406A, a tube voltage of 45 kV, and a tube current of 40 mA, in the range of 5–100° at the speed of 0.05°/min.

Scanning electron microscopy (SEM) was employed to investigate the morphology of the 3D-printed conduits and using Entry-level SEM (Zeiss sigma VP) with an accelerating voltage of 8 kV.

Conductivity along the in-plane direction was measured by the standard four-point probe method using JANDEL (model RM3000) by measuring the resistivity of all PU films. Square films (50 × 50 mm) with uniform thickness were prepared by stereolithography. For each sample, data was collected from five points. The resistivity of the samples were measured according to Eq. (1) [30], and conductivity was calculated according to Eq. (2).

$$\rho = 4.532 \times V/I \times t \tag{1}$$

$$\sigma = \rho^{-1} \tag{2}$$

where ρ is resistivity, V is voltage, I is current, t is the thickness of samples, and σ is conductivity. The conductivity values are calculated and reported in S/cm.

Raman spectroscopy measurement was performed using LabRAM HR UV-NIR and the PARK XE-100 AFM instrument at a wavelength of 514 nm from 500 to 3500 cm^{-1} using an Ar laser source operating.

A commercial SLA device (Formlab 1+) was employed to fabricate all 3D printed tubes including hollow, porous, and grooved conduits. The STL format of the designed tubes was created by 3D CAD software (Robert McNeel and associates). The fabrication process was performed with a 50 mW violet (405 nm) laser beam. The printing resolution was 250 μm in the xy direction and 5 μm per layer.

The contact angle was measured to investigate the hydrophilic/hydrophobic nature of the polymeric films, using a Theta Flex optical tensiometer. Approximately 10 μl of distilled water was dropped onto the surface of the films, and the measurement was conducted on at least five points for each sample.

2.7. *In vitro* enzymatic degradation

The enzymatic degradation of PU and PU/PEG-GO composite films (n = 3) was performed in PBS, pH = 7.4 containing 800 mg/L of Lysozyme at 37 °C in a shaker at 100 rpm. The enzymatic degradation was observed for six weeks, and the lysozyme solution was renewed every three days. At a certain time (every week), samples were removed from the medium, washed with distilled water, and dried in the vacuum oven at 40 °C for 24 h. The weight of the samples was measured before (W_0) and after *in vitro* degradation (W_t). The weight loss was calculated according to Eq. (3).

$$Weightloss[\%] = (W_0 - W_t)/W_0 \times 100 \tag{3}$$

where W_0 is the weight of the sample before degradation and W_t is the weight of the sample at the given time.

3. Results and discussion

One of the desirable features of an ideal NGC is conductivity when it is being considered for peripheral nerve regeneration. Accordingly, the aim of this study was to utilize graphene as a conductive nanofiller to develop proper polymeric composites to be printed into a nerve tube with precise geometry using SLA. In this study, a photo cross-linkable and biocompatible PU resin was synthesized according to our previous study [29] and was used as a polymeric matrix for the development of nerve conduits. To improve the compatibility and dispersity of graphene nanosheets into the PU matrix, it was functionalized through PEGylation reaction (Fig. 1). The PEG functional groups on the surface of the graphene nanosheets were expected to improve the hydrophilicity of the composite, which is an important factor for wettability and cell attachment [31]. In addition, the use of conductive nanofillers can accelerate regeneration of damaged nerves [32]. Finally, the best composition of PU/PEG-GO was selected based on different physicochemical properties that could be printed into nerve conduits with different precise geometries, such as hollow, porous, and grooved tubes

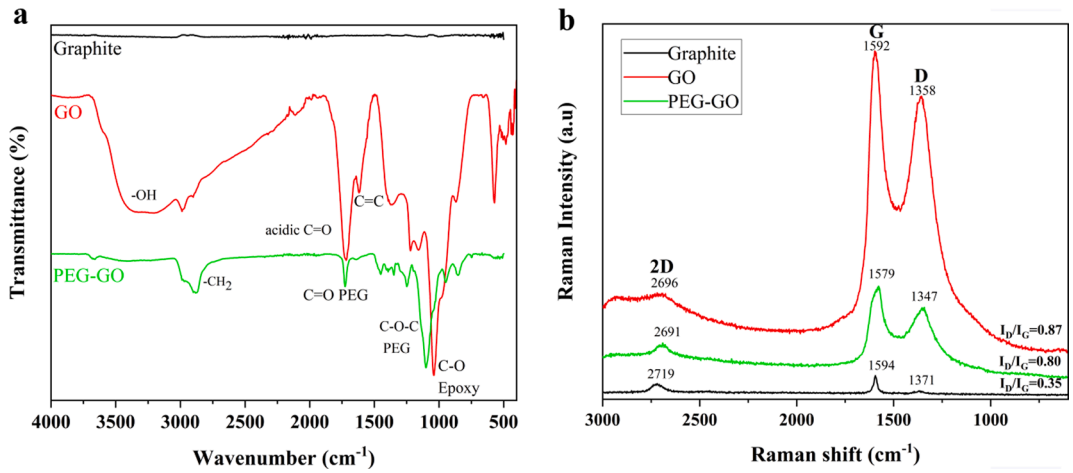

Fig. 2. (a) FTIR spectra of the pure graphite, GO, and PEG-GO and (b) Raman spectra of the pure graphite, GO, and PEG-GO.

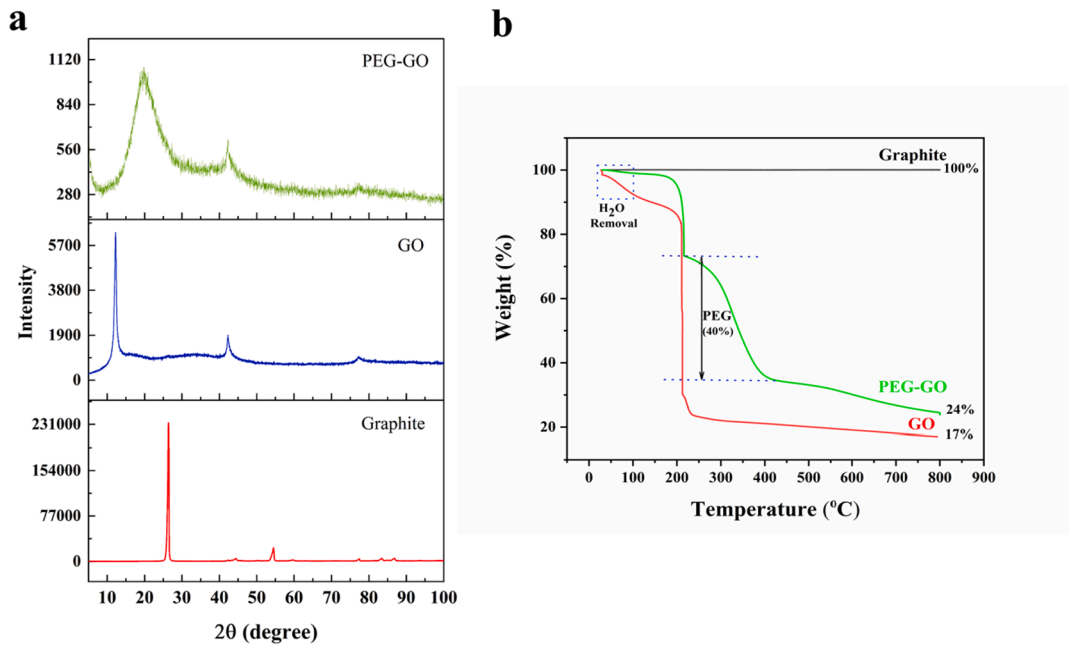

Fig. 3. (a) XRD patterns of the pure graphite, GO, and PEG-GO and (b) TGA thermograms of graphite, GO, and PEG-GO.

(Fig. 1).

3.1. Synthesis of PEG-GO

GO was synthesized through Hummer's method [33], and oxygen-containing groups, such as carboxyl (—COOH), epoxy (—C—O—C—), and hydroxyl (—OH) functionalities, were introduced onto the basal planes as well as on the edges of graphene layers (Fig. 1). Then, GO was PEGylated through radical polymerization of MPEG on its surface. By inserting PEG functional groups, the van der Waals bond between the carbon layers decreases, which can cause exfoliation of graphene layers and more efficiency in graphene dispersion in both protic and non-protic solvents [34]. In addition, according to the literature, PEGylation of GO enhances cytocompatibility [35], cell attachment, and proliferation [36], which are important for the development of materials for tissue engineering. Thus, polymeric composites containing PEG-GO can show promising results in tissue engineering, such as bone [37], skin [38], cardiac [39], and neural [40] tissue engineering.

3.2. Characterization of GO and PEG-GO

3.2.1. FTIR analysis

Bonding interactions and chemical functional groups in natural graphite, GO, and PEG-GO were investigated with the FTIR technique. The FTIR spectra are presented in Fig. 2a. According to the graphite spectrum, there was no specific peak while, in the GO spectrum, there was a peak at 1037 cm^{-1}, which was attributed to the C—O bond, and it supported the existence of the oxide functional group after the oxidation reaction. The peak at 1721 cm^{-1} was related to the acidic carbonyl group, and the peak at 1600 cm^{-1} was attributed to C═C bonds. Furthermore, a broad peak centered at around 3260 cm^{-1} was attributed to the stretching bond of —OH, which was related to the carboxylic acid and hydroxyl functional groups. All these peaks proved that the oxidation was successfully occurred. After GO PEGylation, a peak at 1105 cm^{-1} was observed, which corresponded to the etheric bond of PEG moieties and confirmed successful functionalization of GO with PEG.

3.2.2. Raman spectroscopy

Raman spectroscopy was employed to study the structure of the

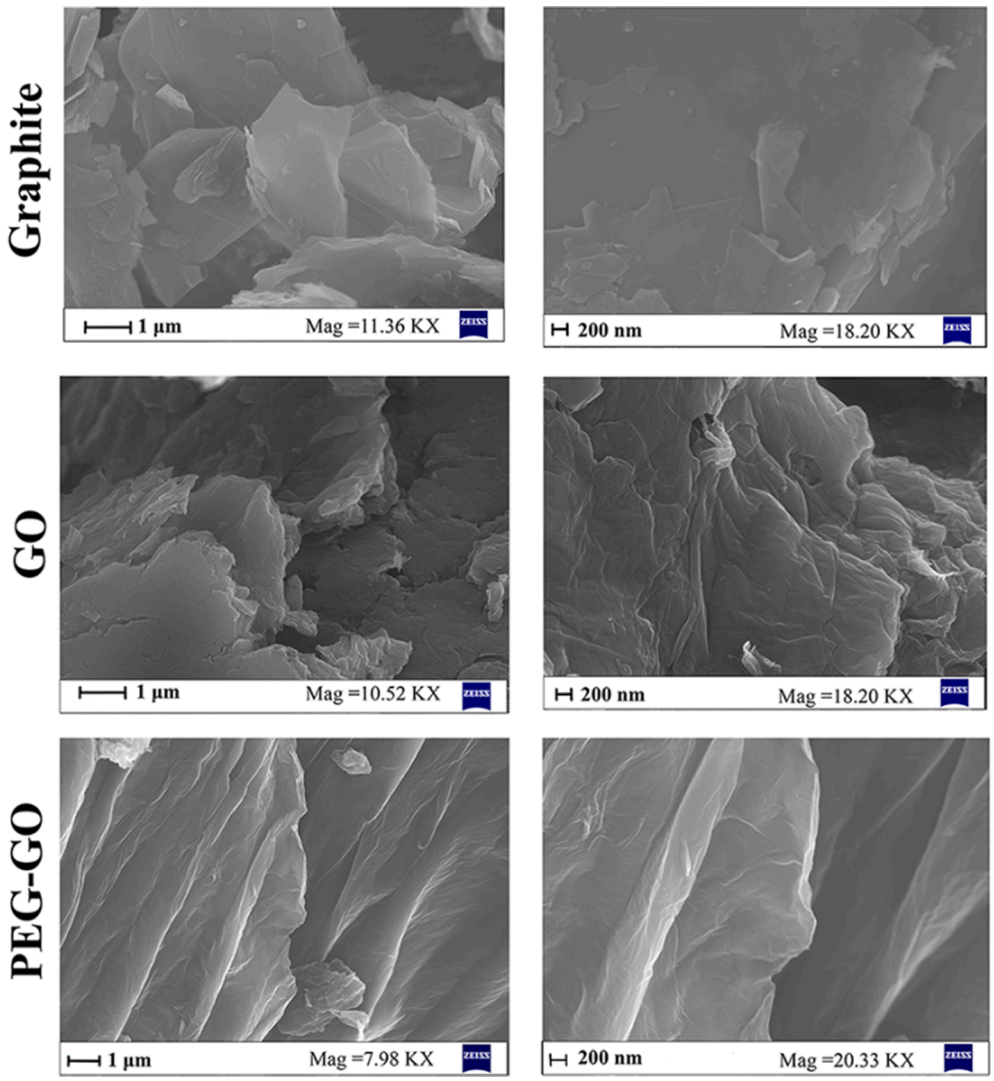

Fig. 4. SEM images of graphite, GO, and PEG-GO.

carbon materials and the changes that have occurred in the graphene structure after oxidation and functionalization. The significant characteristic peaks in the Raman spectra of carbon materials are 2D, D, and G. Generally, in graphitic structures, the G band is attributed to sp^2 carbon atoms in the hexagonal lattice of graphite while the D band, which has a lower intensity, corresponds to the carbon atoms with the configuration of sp^3. The D band is related to the existence of disorders and defects, which are created after oxidation, especially those are located at the edge of graphite sheets [41]. In addition, the Raman spectrum of carbon compounds contains the 2D band, which is attributed to the stacking of graphene sheets. According to the shape of the 2D band, its position and intensity, the formation and the number of layers can be concluded [28]. The Raman spectra of pure graphite, GO, and PEG-GO are presented in Fig. 2b. Based on the intensity ratio of the D and G band (I_D/I_G), the respective carbon atoms with a configuration of sp^3 to sp^2 can be derived. In the graphite Raman spectrum, the I_D/I_G was 0.35, which showed the ratio of sp^2 carbon atoms was predominant. Through an oxidation reaction, the number of sp^2 carbon atoms altered to sp^3 by the insertion of oxygen-containing functional groups onto the graphene basal plane, and as a result, the I_D/I_G increased to 0.87. The I_D/I_G for PEG-GO was 0.80, which indicated an almost similar degree of disorder compared to GO. These results revealed that functionalization of GO significantly occurred on the defect sites of the GO surface; thus, the ratio of sp^3 to sp^2 remained constant and did not change through insertion of PEG onto the surface [42].

3.2.3. XRD studies

Fig. 3a illustrates the XRD patterns of pure graphite, GO, and PEG-GO. The prominent peak of graphite at $2\theta = 26.6^{\circ}$ matched with the (0 0 2) reflection plane. This implied that graphite is a well-aligned carbon material. In addition, the XRD pattern of GO exhibited a significant peak at 11.6°, which showed the layer-to-layer distance of GO sheets was higher than graphite. This observation confirmed the insertion of functional groups on the surface of planes in GO, which resulted in an increase in inter-layer spacing [43]. For PEG-GO, a broad peak was observed at $2\theta = 19.8^{\circ}$, which confirmed that PEG was inserted on the surface of GO and the distance of the graphene sheets had been changed due to the interaction of PEG moieties between graphene layers.

3.2.4. Thermal properties

The thermal properties of the pure graphite, GO, and PEG-GO were investigated using the TGA technique. The results are shown in Fig. 3b. According to the results, there was no significant changes for the percent of weight loss of graphite until 800 °C, while two and three important decomposition temperatures were observed for GO and PEG-GO, respectively. The first weight loss for both GO and PEG-GO was related to the evaporation of water. The second weight loss at around 250 °C was related to the pyrolysis of functional groups, which contain

Fig. 5. Contact angle images of PU films with different amounts of PEG-GO.

Table 1
Contact angle results of polymeric films containing various amount of PEG-GO.

Sample	PU/PEG-GO 0%	PU/PEG-GO 0.5%	PU/PEG-GO 1%	PU/PEG-GO 3%	PU/PEG-GO 5%
Contact angle	~ 103°	77°	76°	73°	72°

Table 2
Young modulus, tensile stress, and tensile strain at break of PU composites containing different amounts of PEG-GO (n = 5, average ± SD).

Sample	Young Modulus (MPa)	Tensile stress (MPa)	Tensile strain (%)
PU/PEG-GO 0%	4.48 ± 0.10	3.33 ± 0.25	145.00 ± 7.60
PU/PEG-GO 0.5%	3.36 ± 0.06	2.50 ± 0.01	127.15 ± 16.79
PU/PEG-GO 1%	3.29 ± 0.04	2.52 ± 0.07	124.32 ± 6.11
PU/PEG-GO 3%	2.97 ± 0.40	2.48 ± 0.11	140.08 ± 8.22
PU/PEG-GO 5%	2.52 ± 0.14	3.51 ± 0.54	169.33 ± 12.19

oxygen (i.e., epoxy groups, carboxyl, and hydroxyl groups) [44]. The weight loss of PEG-GO was more moderate than GO, especially in the temperature range of 40–220 °C, suggesting a decrease in the amount of oxygen-containing functional groups after functionalization with PEG. In addition, in the TGA thermogram of PEG-GO, a new weight loss (~40%) was observed in the temperature range of 200–400 °C, attributable to the degradation of grafted PEG chains, which confirmed the functionalization of GO with PEG.

3.2.5. SEM images

SEM analysis was utilized to study the morphology of pure graphite, GO, and PEG-GO as well as the thickness of the layers and distance between them. All samples are illustrated in Fig. 4 at different magnifications. According to the SEM images, all samples showed sheet-like structures. For the GO sample, the existence of folded layers with several wrinkles proved the interaction between the oxygen-containing functional groups in this structure. The SEM image of PEG-GO exhibited a higher distance between layers compared with GO. This phenomenon could have occurred due to the interaction of PEG moieties between GO layers. In addition, the number of layers was reduced after the PEGylation of GO; this fact can be further proved with the thin, more transparent, and paper-like structure of PEG-GO, which was due to the reduction of the oxygen-containing functional groups on the surface of GO after the PEGylation reaction.

3.3. Characterization of composite

3.3.1. Contact angle

Hydrophilicity/hydrophobicity of the polymeric samples is a key

Table 3
Conductive properties of films containing PEG-GO.

Sample	PU/PEG-GO 0%	PU/PEG-GO 0.5%	PU/PEG-GO 1%	PU/PEG-GO 3%	PU/PEG-GO 5%
Conductivity (S/cm)	4.1×10^{-11}	5.2×10^{-5}	1.4×10^{-4}	3.1×10^{-4}	1.1×10^{-3}

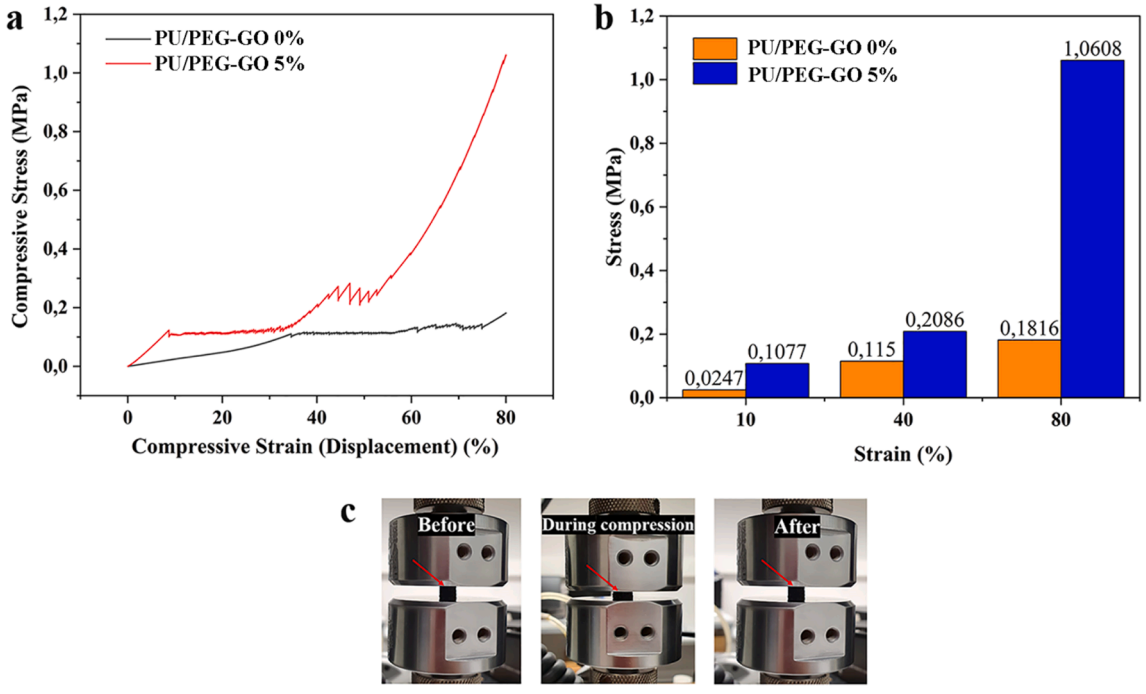

Fig. 6. (a) compressive stress–strain graph, (b) compressive stress at different strain level, and (c) photographs of cylindrical printed structure before, during, and after compression.

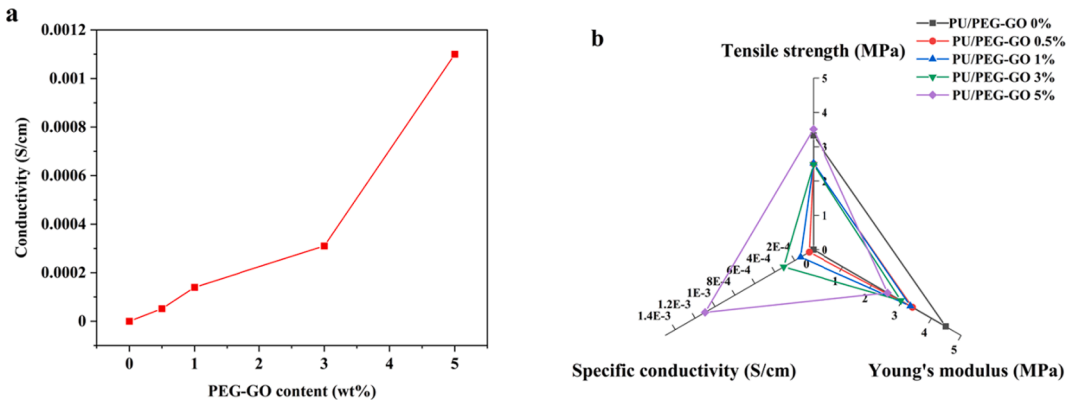

Fig. 7. (a) Conductivity and (b) property profile of pure PU and PU/PEG-GO composites.

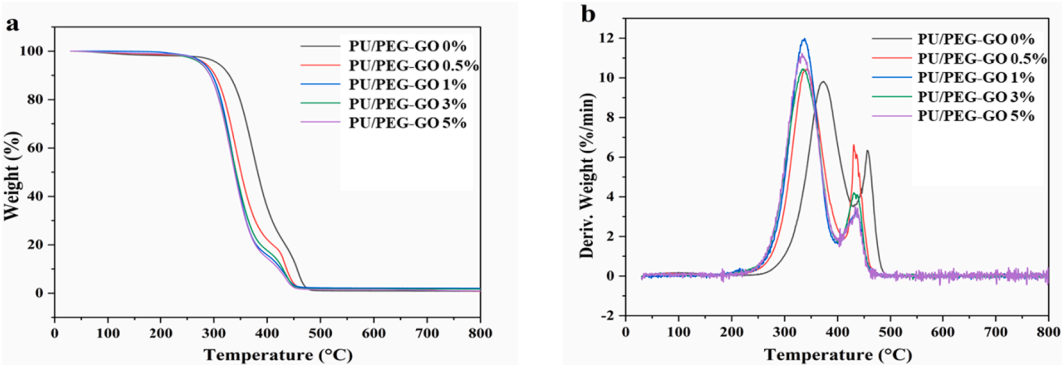

Fig. 8. (a) TGA and (b) DTG thermograms of PU samples.

Table 4
TGA data for PU and PU films contain PEG-GO.

Sample	$T_{5\%}$ (°C)	$T_{10\%}$ (°C)	$Tmax_1$ (°C)	$Tmax_2$ (°C)
PU/PEG-GO 0%	305.4	328.2	373.4	456.8
PU/PEG-GO 0.5%	282.9	302.3	342.8	430.4
PU/PEG-GO 1%	278.3	296.2	337.8	434.1
PU/PEG-GO 3%	274.2	292.6	333.9	430.6
PU/PEG-GO 5%	275.9	292.6	332.8	433.2

characteristic feature for attachment of cells on the surface of materials, which can be measured by contact angle technique. According to the literature, the contact angle of the materials in the range of 40° to 80° has been shown to provide the best range for cell adhesion of multiple cell types [45]. The contact angles of PU films with different amounts of PEG-GO are shown in Fig. 5 and Table 1. According to the results, the PU film containing 0% PEG-GO showed the highest contact angle (~103°), and the samples with 5% PEG-GO showed the lowest contact angle (~72°). It was hypothesized that PEGylation of GO provided many hydrophilic groups on its surface, leading to increase the hydrophilicity of the composite containing higher PEG-GO content and its conduit. owing to the hydrophilic nature of the PEG-GO particles. According to the literature, nerve cells have a high affinity to attach and proliferate on more hydrophilic surfaces [46]. Therefore, among all the samples, it is expected that the PU/PEG-GO 5% will show better results for cell attachment and cell proliferation, which can lead to an acceleration in the nerve regeneration process.

3.3.2. *Mechanical properties*

Mechanical performance is one of the key features of materials in tissue engineering application. The mechanical tensile test results of pure PU and PU/PEG-GO composites are presented in Table 2. The tensile test was performed with a pulling rate of 10 mm/min. The difference in the content of PEG-GO in the PU samples caused significant changes in the mechanical properties. Among all the samples, PU/PEG-GO 5% showed the highest tensile stress (3.51 ± 0.54 MPa) and tensile strain at break (~170%). Another mechanical property is the Young modulus, which shows the tensile stiffness of the material. Based on the results, the PU film containing 5% PEG-GO exhibited the lowest stiffness (2.52 ± 0.14 MPa). Generally, according to the literature for the application of nerve regeneration, mechanical strength should be in the range of between 0.3 and 30 MPa [14,47]. Thus, the mechanical properties of this sample would be suitable for soft tissue engineering applications [48].

To evaluate the mechanical properties of the PU composite containing 5% PEG-GO, which is the selected sample for 3D printing, a compressive test was performed on the printed cylindrical porous structure, and the results compared with a sample containing 0% PEG-GO. The compressive stress strain graph is presented in Fig. 6a. In addition, the stress at different strain levels is shown in Fig. 6b, and photographs of the cylindrical 3D-printed structure before, during compression, and after recovery are illustrated in Fig. 6c. The samples showed excellent stability during the test and were not torn nor collapsed. The sample containing 0% PEG-GO presented an almost linear trend with a mild slope in the stress–strain curve up to 80% strain. It did not show a sharp increase in stress value even after 80% displacement. In contrast, the sample containing 5% PEG-GO presented a sharp increase after 50% strain, and the stress value reached 1.06 MPa at 80% strain. According to the results, a significant improvement was observed for samples containing 5% PEG-GO in terms of their compression mechanical properties. A comparison of the stress value for both samples at different levels of strain shows that at 10%, 40%, and 80% of strain, the deformation for the sample containing 5% PEG-GO is more difficult than the sample containing 0% PEG-GO.

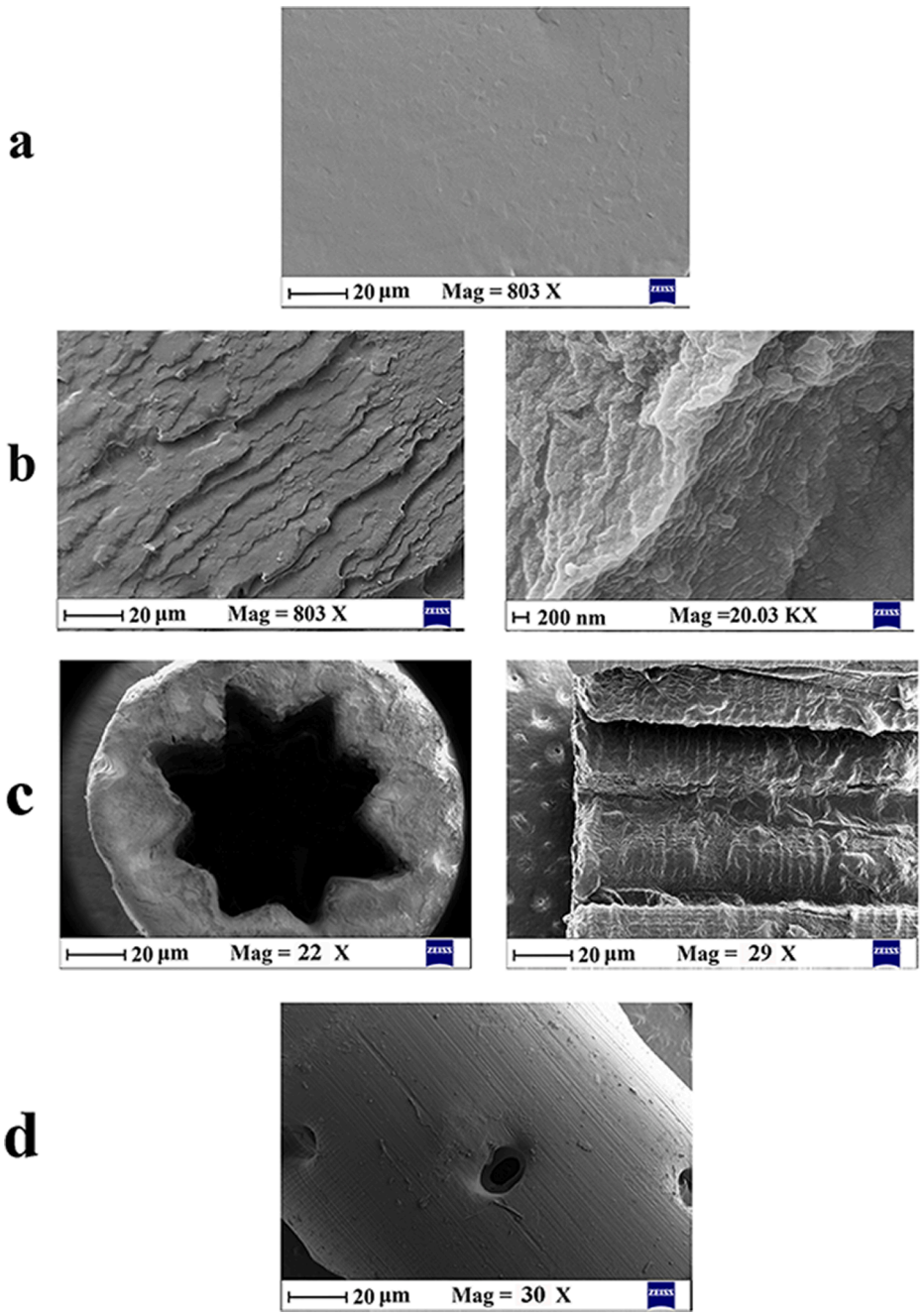

Fig. 9. SEM cross-section images of (a) pure PU, (b) PU/PEG-GO 5%, (c) cross section (left) and longitudinal section (right) SEM images of grooved 3D-printed conduit, and (d) SEM cross-section image of porous 3D-printed conduit manufactured by SLA and using PU/PEG-GO 5%.

3.3.3. *Conductivity*

The application of conductive materials for the fabrication of nerve conduits can stimulate cellular function, and it would likely be promising for the regeneration of damaged peripheral nerves [49,50]. In this study, the electrical conductivity results of composites showed that by adding PEG-GO as a conductive particle into PU, conductivity can be induced in the samples. As presented in Table 3, along with increasing the PEG-GO content into the PU matrix, conductivity was gradually increased, and the polymer composite was converted from an insulator (neat PU with conductivity of $\sim 10^{-11}$ S/cm) to conductor. As shown in Fig. 7a, the percolation threshold was reached after the loading of PEG-GO at between 3 and 5 wt%, and it is due to the formation of multiple conducting networks [51]. The percolation threshold depends on the dispersion state of the filler into the main matrix of the polymer [52]. A conductivity of 1.1×10^{-3} S/cm was measured for the film containing 5 wt% of PEG-GO, which is suitable for the application of nerve conduits [52]. Fig. 7b also displays a comparison between Young's modulus, tensile strength, and conductivity of all samples and clearly showed that PU/PEG-GO 5% had better property profile compared with others.

3.3.4. *TGA results*

The TGA technique was utilized to investigate the thermal stability of the synthesized composites. The weight loss (TG) and derivative weight loss diagrams of the samples are illustrated in Fig. 8a and b respectively. The corresponding data according to the TGA thermograms for the degradation temperature at 5, 10, and maximum weight loss (T5%, T10%, $Tmax_1$, and $Tmax_2$) are presented in Table 4. The thermal degradation of all prepared PU composites proceeded in two major

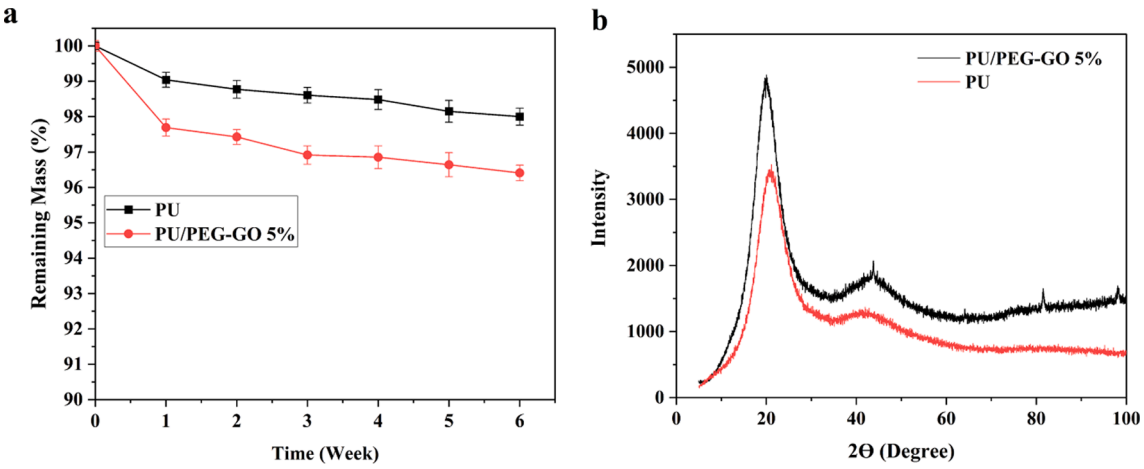

Fig. 10. (a) Enzymatic degradation and (b) XRD patterns of pure PU and PU/PEG-GO 5% composite.

steps. The first weight loss step ($Tmax_1$) for all samples was observed in the range of 330 °C to 380 °C which is related to the decomposition of urethane, ether, and/or ester groups [53]. Moreover, the first weight loss for PU/PEG-GO composites was initiated at a lower temperature compared with pure PU, which can be due to the decomposition of the PEG functional groups at the surface of PEG-GO. The second weight loss ($Tmax_2$), which was occurred between 430 °C and 460 °C was related to the breaking of C-C bonds [53]. In addition, by increasing the amount of PEG-GO, the thermal stability of the samples gradually decreased from PU/PEG-GO 0.5% to PU/PEG-GO 5%, which may be due to the lack of thermal stability of the etheric bonds of grafted PEG chains on the surface of GO compared with the esteric bonds of PU [54].

3.3.5. SEM images

The final properties, functionality, and quality of the nanocomposite can be affected by the dispersion, homogeneity, and compatibility of the nanoparticles in the polymer matrix. The SEM technique was used in this study to investigate the influence of PEGylation of GO on its properties for the quality of dispersion in the polymer matrix and its compatibility with PU. According to the conductivity results, and the mechanical, thermal, and surface properties, the PU composite containing 5% PEG-GO was selected for the 3D printing of nerve conduits. Therefore, SEM images for the composite was taken for this sample and compared with pure PU. The SEM cross-section images of pure PU and PU/PEG-GO 5% composite films at different magnifications are illustrated in Fig. 9a and 9b. The homogeneous dispersion of PEG-GO sheets in the PU matrix was observed in PU/PEG-GO 5% (Fig. 9b), confirming perfect interfacial interaction of the functionalized graphene layers with PU. Thus, good compatibility between the different phases resulted from PEGylation of GO. Moreover, the SEM images of 3D-printed nerve conduits, grooved and porous tubes, manufactured by SLA and using PU/PEG-GO 5% are shown in Fig. 9c and d. Cross section (left) and longitudinal section (right) images of grooved tube are displayed in Fig. 9c, demonstrating the presence of aligned grooves in the z-axis direction. The longitudinal section image of printed nerve conduit (Fig. 9c, right) clearly exhibited well dispersion of PEG-GO in the polymer matrix without any aggregation.

3.3.6. Enzymatic degradation

Enzymatic degradation is another important feature for implantable materials in tissue engineering that can affect the overall efficiency. The lifetime of the tissue scaffold should be adjusted according to the time required for regeneration of the organ; it would vary from weeks to months. Therefore, the *in vitro* enzymatic degradation was evaluated for the targeted sample for the fabrication of conduits, PU/PEG-GO 5%, and the results were compared with pure PU. The degradation graphs of pure PU and PU/PEG-GO 5% for 6 weeks are shown in Fig. 10a. Both pure PU and PU/PEG-GO 5% showed higher degradation at first week. The weight loss was around 1% for pure PU and 2.3% for PU containing 5% PEG-GO. Then the degradation rates of both samples slowed down after 1 week and gradual degradation rate was seen until week 6. At the end of the test at week 6, PU and PU/PEG-GO 5% exhibited 2% and 3.5% weight loss, respectively. The PU/PEG-GO 5% showed a faster degradation rate, ranging from 2.3% to 3.5% for 6 weeks. The most important reason for faster degradation of the composite containing 5% PEG-GO can be attributed to its hydrophilicity, which caused more enzyme solution to access the bulk structure, resulting in an increase in hydrolytic degradation. According to the literature, approximately 6–12 weeks are needed for a complete nerve regeneration, depending on the severity [55]. Therefore, the degradation rate of a proper nerve conduit should be in this range to allow efficient nerve repair. According to the obtained results, the developed PU/PEG-GO 5% conduit showed 96% of residual weights by the end of week 6, demonstrating that the conduit can maintain its structure until the efficient regeneration of nerve tissue.

3.3.7. XRD studies for composite

Fig. 10b illustrates the XRD patterns of the PU films containing 0% and 5% PEG-GO to investigate the crystalline behavior of the samples. For each sample, two significant peaks were observed at $2\Theta = 21^{\circ}$ and $2\Theta = 45^{\circ}$ which were related to the PU polymer and confirmed the amorphous structure of the polymer. In addition, two small sharp peaks were observed in the diffractometer of the composite containing 5% PEG-GO at around $2\Theta = 45^{\circ}$ and $2\Theta = 80^{\circ}$, which were existed in XRD graph of pure PEG-GO (Fig. 3a), and it can confirm incorporation of PEG-GO into the PU matrix. Generally, the amorphous structure of the PU is because of the presence of PCL moieties in the PU structure and the addition of PEG-GO does not have a significant effect on the amorphous structure of the polymer. Being amorphous would be important for the degradation rate of the composite because amorphous structures are highly prone to decomposition, and this parameter is essential for tissue engineering applications [56].

4. Conclusion

Proper materials and fabrication technique were designed and developed to achieve desired properties of an ideal conduit for peripheral nerve repair. To this aim, a biocompatible, photo-crosslinkable and solvent-free PU was used as a matrix and functionalized GO was used as a conductive nanofiller. To reduce GO cytotoxicity and to improve its compatibility with PU, it was PEGylated through radical polymerization. The composites were prepared using solvent-free PU and different contents of PEG-GO (0, 0.5, 1, 3, and 5 wt%). The addition of 5 wt%

PEG-GO significantly increased the conductivity into a proper range for the application of nerve conduits. The composite containing 5% PEG-GO exhibited the highest tensile stress (3.51 ± 0.54 MPa), tensile strain at break (~170%), and compression strength thanks to the homogeneous dispersion of PEG-GO in the polymer matrix arising from surface modification of GO. Finally, 3D-printed nerve conduits were designed and developed with different precise geometries, including hollow, porous, and grooved tubes using SLA and PU/PEG-GO 5%. The developed PU/PEG-GO 5% conduit showed 96% of residual weights by the end of week 6, demonstrating that the conduit maintained its structure until the proper regeneration of nerve tissue. We believe that a combination of various parameters, such as using PU/PEG-GO composite with controlled physicochemical properties and applying different precise geometries through 3D printing technique, ultimately led to the best results of developing ideal nerve conduit. In our opinion, the developed 3D-printed conduit has potential to be used as NGCs for peripheral nerve injury repair; however, more research is still needed to be done for analyzing the newly developed conduits in detail *in vitro* and *in vivo* before clinical use.

CRediT authorship contribution statement

Afsoon Farzan: Conceptualization, Methodology, Validation, Formal analysis, Investigation, Resources, Writing – original draft. **Sedigheh Borandeh:** Conceptualization, Formal analysis, Investigation, Writing – original draft, Writing – review & editing. **Jukka Seppälä:** Supervision, Funding acquisition.

Declaration of Competing Interest

The authors declare that they have no known competing financial interests or personal relationships that could have appeared to influence the work reported in this paper.

Acknowledgment

The authors would like to thank the Magnus Ehrnrooth Foundation, Finnish Cultural Foundation, and Academy of Finland No. 307485 (3D-Biomat) for providing funding for this project. This work made use of the BIOECONOMY infrastructure at Aalto University.

References

[1] H. Xu, J.M. Holzwarth, Y. Yan, P. Xu, H. Zheng, Y. Yin, S. Li, P.X. Ma, Conductive PPY/PDLLA conduit for peripheral nerve regeneration, Biomaterials 35 (1) (2014) 225–235, https://doi.org/10.1016/j.biomaterials.2013.10.002.

[2] M.G. Burnett, E.L. Zager, Pathophysiology of peripheral nerve injury: a brief review, Neurosurg. Focus. 16 (5) (2004) 1–7, https://doi.org/10.3171/foc.2004.16.5.2.

[3] M. Reichenberger, E. Gazyakan, S. Kohler, G. Germann, H. Engel, A new, custom-made device for flap protection in experimental rats, Microsurg.: Off. J. Int. Microsurg. Soc. Eur. Federat. Soc. Microsurg. 29 (6) (2009) 504–506.

[4] P. Scherman, M. Kanje, L.B. Dahlin, Bridging short nerve defects by direct repair under tension, nerve grafts or longitudinal sutures, Restor. Neurol. Neurosci. 22 (2004) 65–72.

[5] A. Singh, S. Asikainen, A.K. Teotia, P.A. Shiekh, E. Huotilainen, I. Qayoom, J. Partanen, J. Seppälä, A. Kumar, Biomimetic photocurable three-dimensional printed nerve guidance channels with aligned cryomatrix lumen for peripheral nerve regeneration, ACS Appl. Mater. Interf. 10 (2018) 43327–43342, https://doi.org/10.1021/acsami.8b11677.

[6] R. Deumens, A. Bozkurt, M.F. Meek, M.A.E. Marcus, E.A.J. Joosten, J. Weis, G. A. Brook, Repairing injured peripheral nerves: Bridging the gap, Prog. Neurobiol. 92 (3) (2010) 245–276, https://doi.org/10.1016/j.pneurobio.2010.10.002.

[7] S. Wang, L. Cai, Polymers for fabricating nerve conduits, Int. J. Polym. Sci. 2010 (2010) 1–20, https://doi.org/10.1155/2010/138686.

[8] S.-H. Hsu, W.-C. Chang, C.-T. Yen, Novel flexible nerve conduits made of water-based biodegradable polyurethane for peripheral nerve regeneration, J. Biomed. Mater. Res. - Part A. 105 (5) (2017) 1383–1392, https://doi.org/10.1002/jbm.a.36022.

[9] S.A. Guelcher, K.M. Gallagher, J.E. Didier, D.B. Klinedinst, J.S. Doctor, A. S. Goldstein, G.L. Wilkes, E.J. Beckman, J.O. Hollinger, Synthesis of biocompatible segmented polyurethanes from aliphatic diisocyanates and diurea diol chain extenders, Acta Biomater. 1 (4) (2005) 471–484, https://doi.org/10.1016/j.actbio.2005.02.007.

[10] Y. Niu, L. Li, K.C. Chen, F. Chen, X. Liu, J. Ye, W. Li, K. Xu, Scaffolds from alternating block polyurethanes of poly(ε-caprolactone) and poly(ethylene glycol) with stimulation and guidance of nerve growth and better nerve repair than autograft, J. Biomed. Mater. Res. - Part A. 103 (2015) 2355–2364, https://doi.org/10.1002/jbm.a.35372.

[11] Y. Niu, K.C. Chen, T. He, W. Yu, S. Huang, K. Xu, Scaffolds from block polyurethanes based on poly(ε-caprolactone) (PCL) and poly(ethylene glycol) (PEG) for peripheral nerve regeneration, Biomaterials 35 (2014) 4266–4277, https://doi.org/10.1016/j.biomaterials.2014.02.013.

[12] D. Yin, X. Wang, Y. Yan, R. Zhang, Preliminary studies on peripheral nerve regeneration using a new polyurethane conduit, J. Bioact. Compat. Polym. 22 (2007) 143–159, https://doi.org/10.1177/0883911506076063.

[13] T. Cui, X. Wang, Y. Tan, R. Zhang, Rapid prototyping a double-layer polyurethane-collagen conduit and its Schwann cell compatibility, J. Bioact. Compat. Polym. 24 (1_suppl) (2009) 5–17, https://doi.org/10.1177/0883911509102349.

[14] V. Chiono, C. Tonda-Turo, Trends in the design of nerve guidance channels in peripheral nerve tissue engineering, Prog. Neurobiol. 131 (2015) 87–104, https://doi.org/10.1016/j.pneurobio.2015.06.001.

[15] F.P.W. Melchels, J. Feijen, D.W. Grijpma, A review on stereolithography and its applications in biomedical engineering, Biomaterials 31 (24) (2010) 6121–6130, https://doi.org/10.1016/j.biomaterials.2010.04.050.

[16] D. Yucel, G.T. Kose, V. Hasirci, Polyester based nerve guidance conduit design, Biomaterials. 31 (7) (2010) 1596–1603, https://doi.org/10.1016/j.biomaterials.2009.11.013.

[17] S.A. Mobasseri, G. Terenghi, S. Downes, Micro-structural geometry of thin films intended for the inner lumen of nerve conduits affects nerve repair, J. Mater. Sci. Mater. Med. 24 (7) (2013) 1639–1647, https://doi.org/10.1007/s10856-013-4922-5.

[18] T. Gordon, Electrical stimulation to enhance axon regeneration after peripheral nerve injuries in animal models and humans, Neurotherapeutics 13 (2) (2016) 295–310, https://doi.org/10.1007/s13311-015-0415-1.

[19] X. Hu, X. Wang, Y. Xu, L. Li, J. Liu, Y. He, Y. Zou, L. Yu, X. Qiu, J. Guo, Electric conductivity on aligned nanofibers facilitates the transdifferentiation of mesenchymal stem cells into Schwann cells and regeneration of injured peripheral nerve, Adv. Healthc. Mater. 9 (11) (2020) 1901570, https://doi.org/10.1002/adhm.v9.1110.1002/adhm.201901570.

[20] B. Guo, P.X. Ma, Conducting polymers for tissue engineering, Biomacromolecules 19 (6) (2018) 1764–1782, https://doi.org/10.1021/acs.biomac.8b00276.

[21] R. Balint, N.J. Cassidy, S.H. Cartmell, Conductive polymers: Towards a smart biomaterial for tissue engineering, Acta Biomater. 10 (6) (2014) 2341–2353, https://doi.org/10.1016/j.actbio.2014.02.015.

[22] B. Huang, Carbon nanotubes and their polymeric composites: the applications in tissue engineering, Biomanu. Rev. 5 (2020) 1–26, https://doi.org/10.1007/s40898-020-00009-x.

[23] H.o. Bei, Y. Yang, Q. Zhang, Y.u. Tian, X. Luo, M.o. Yang, X. Zhao, Graphene-based nanocomposites for neural tissue engineering, Molecules 24 (4) (2019) 658, https://doi.org/10.3390/molecules24040658.

[24] I. Chowdhury, N.D. Mansukhani, L.M. Guiney, M.C. Hersam, D. Bouchard, Aggregation and stability of reduced graphene oxide: complex roles of divalent cations, pH, and natural organic matter, Environ. Sci. Technol. 49 (18) (2015) 10886–10893, https://doi.org/10.1021/acs.est.5b01866.

[25] S.H. Ku, M. Lee, C.B. Park, Carbon-based nanomaterials for tissue engineering, Adv. Healthc. Mater. 2 (2) (2013) 244–260, https://doi.org/10.1002/adhm.201200307.

[26] M. Xu, J. Zhu, F. Wang, Y. Xiong, Y. Wu, Q. Wang, J. Weng, Z. Zhang, W. Chen, S. Liu, Improved in vitro and in vivo biocompatibility of graphene oxide through surface modification: poly(acrylic acid)-functionalization is superior to PEGylation, ACS Nano. 10 (2016) 3267–3281, https://doi.org/10.1021/acsnano.6b00539.

[27] S. Ghosh, K. Chatterjee, Poly(Ethylene glycol) functionalized graphene oxide in tissue engineering: a review on recent advances, Int. J. Nanomed. 15 (2020) 5991–6006, https://doi.org/10.2147/IJN.S249717.

[28] S. Mallakpour, A. Abdolmaleki, S. Borandeh, Covalently functionalized graphene sheets with biocompatible natural amino acids, Appl. Surf. Sci. 307 (2014) 533–542, https://doi.org/10.1016/j.apsusc.2014.04.070.

[29] A. Farzan, S. Borandeh, N. Zanjanizadeh Ezazi, S. Lipponen, H.A. Santos, J. Seppälä, 3D scaffolding of fast photocurable polyurethane for soft tissue engineering by stereolithography: Influence of materials and geometry on growth of fibroblast cells, Eur. Polym. J. 139 (2020) 109988, https://doi.org/10.1016/j.eurpolymj.2020.109988.

[30] B. Subramanian, M. Mohamed Ibrahim, V. Senthilkumar, K.R. Murali, V.S. Vidhya, C. Sanjeeviraja, M. Jayachandran, Optoelectronic and electrochemical properties of nickel oxide (NiO) films deposited by DC reactive magnetron sputtering, Phys. B Condens. Matter. 403 (21-22) (2008) 4104–4110.

[31] S. Cai, C. Wu, W. Yang, W. Liang, H. Yu, L. Liu, Recent advance in surface modification for regulating cell adhesion and behaviors, Nanotechnol. Rev. 9 (2020) 971–989, https://doi.org/10.1515/ntrev-2020-0076.

[32] C. Dong, F. Qiao, W. Hou, L. Yang, Y. Lv, Graphene-based conductive fibrous scaffold boosts sciatic nerve regeneration and functional recovery upon electrical stimulation, Appl. Mater. Today. 21 (2020) 100870.

[33] W.S. Hummers, R.E. Offeman, Preparation of graphitic oxide, J. Am. Chem. Soc. 80 (1958) 1339, https://doi.org/10.1021/ja01539a017.

[34] S. Zhang, P. Xiong, X. Yang, X. Wang, Novel PEG functionalized graphene nanosheets: enhancement of dispersibility and thermal stability, Nanoscale 3 (2011) 2169–2174, https://doi.org/10.1039/c0nr00923g.

[35] K. Wang, K. Wang, J. Ruan, H. Song, J. Zhang, Y. Wo, S. Guo, D. Cui, Biocompatibility of graphene oxide biocompatibility of graphene oxide, Nanoscale Res Lett. 6 (2010) 8. http://www.nanoscalereslett.com/content/6/1/8.
[36] Q. Liu, J. Shi, J. Sun, T. Wang, L. Zeng, G. Jiang, Graphene and graphene oxide sheets supported on silica as versatile and high-performance adsorbents for solid-phase extraction, Angew. Chemie 123 (26) (2011) 6035–6039, https://doi.org/10.1002/ange.201007138.
[37] A.M. Díez-Pascual, A.L. Díez-Vicente, Poly(propylene fumarate)/polyethylene glycol-modified graphene oxide nanocomposites for tissue engineering, ACS Appl. Mater. Interf. 8 (2016) 17902–17914, https://doi.org/10.1021/acsami.6b05635.
[38] J. Chu, P. Shi, W. Yan, J. Fu, Z. Yang, C. He, X. Deng, H. Liu, PEGylated graphene oxide-mediated quercetin-modified collagen hybrid scaffold for enhancement of MSCs differentiation potential and diabetic wound healing, Nanoscale 10 (20) (2018) 9547–9560.
[39] A.S.T. Smith, H. Yoo, H. Yi, E.H. Ahn, J.H. Lee, G. Shao, E. Nagornyak, M. A. Laflamme, C.E. Murry, D.-H. Kim, Micro-and nano-patterned conductive graphene-PEG hybrid scaffolds for cardiac tissue engineering, Chem. Commun. 53 (53) (2017) 7412–7415.
[40] N. Li, X. Zhang, Q. Song, R. Su, Q.i. Zhang, T. Kong, L. Liu, G. Jin, M. Tang, G. Cheng, The promotion of neurite sprouting and outgrowth of mouse hippocampal cells in culture by graphene substrates, Biomaterials 32 (35) (2011) 9374–9382, https://doi.org/10.1016/j.biomaterials.2011.08.065.
[41] K.N. Kudin, B. Ozbas, H.C. Schniepp, R.K. Prud'homme, I.A. Aksay, R. Car, Raman spectra of graphite oxide and functionalized graphene sheets, Nano Lett. 8 (1) (2008) 36–41, https://doi.org/10.1021/nl071822y.
[42] M. Monajati, S. Borandeh, A. Hesami, D. Mansouri, A.M. Tamaddon, Immobilization of L-asparaginase on aspartic acid functionalized graphene oxide nanosheet: enzyme kinetics and stability studies, Chem. Eng. J. 354 (2018) 1153–1163, https://doi.org/10.1016/j.cej.2018.08.058.
[43] N.I. Kovtyukhova, P.J. Ollivier, B.R. Martin, T.E. Mallouk, S.A. Chizhik, E. V. Buzaneva, A.D. Gorchinskiy, Layer-by-layer assembly of ultrathin composite films from micron-sized graphite oxide sheets and polycations, Chem. Mater. 11 (3) (1999) 771–778, https://doi.org/10.1021/cm981085u.
[44] F.-P. Du, J.-J. Wang, C.-Y. Tang, C.-P. Tsui, X.-P. Zhou, X.-L. Xie, Y.-G. Liao, Water-soluble graphene grafted by poly(sodium 4-styrenesulfonate) for enhancement of electric capacitance, Nanotechnology 23 (47) (2012) 475704, https://doi.org/10.1088/0957-4484/23/47/475704.
[45] T.J. Rivers, T.W. Hudson, C.E. Schmidt, Synthesis of a novel, biodegradable electrically conducting polymer for biomedical applications, Adv. Funct. Mater. 12 (2002) 33–37, https://doi.org/10.1002/1616-3028(20020101)12:1<33::AID-ADFM33>3.0.CO;2-E.
[46] M. Cheng, W. Cao, Y. Gao, Y. Gong, N. Zhao, X. Zhang, Studies on nerve cell affinity of biodegradable modified chitosan films, J. Biomater. Sci. Polym. Ed. 14 (10) (2003) 1155–1167, https://doi.org/10.1163/156856203769231628.
[47] A. Singh, P.A. Shiekh, M. Das, J. Seppälä, A. Kumar, Aligned chitosan-gelatin cryogel-filled polyurethane nerve guidance channel for neural tissue engineering: fabrication, characterization, and in vitro evaluation, Biomacromolecules 20 (2) (2019) 662–673, https://doi.org/10.1021/acs.biomac.8b01308.
[48] W. Zhu, K.R. Tringale, S.A. Woller, S. You, S. Johnson, H. Shen, J. Schimelman, M. Whitney, J. Steinauer, W. Xu, T.L. Yaksh, Q.T. Nguyen, S. Chen, Rapid continuous 3D printing of customizable peripheral nerve guidance conduits, Mater. Today 21 (9) (2018) 951–959, https://doi.org/10.1016/j.mattod.2018.04.001.
[49] P. Zarrintaj, E. Zangene, S. Manouchehri, L.M. Amirabad, N. Baheiraei, M. R. Hadjighasem, M. Farokhi, M.R. Ganjali, B.W. Walker, M.R. Saeb, M. Mozafari, S. Thomas, N. Annabi, Conductive biomaterials as nerve conduits: recent advances and future challenges, Appl. Mater. Today 20 (2020) 100784, https://doi.org/10.1016/j.apmt.2020.100784.
[50] A.A. Al-Majed, C.M. Neumann, T.M. Brushart, T. Gordon, Brief electrical stimulation promotes the speed and accuracy of motor axonal regeneration, J. Neurosci. 20 (7) (2000) 2602–2608.
[51] J. Li, J.-K. Kim, Percolation threshold of conducting polymer composites containing 3D randomly distributed graphite nanoplatelets, Compos. Sci. Technol. 67 (10) (2007) 2114–2120, https://doi.org/10.1016/j.compscitech.2006.11.010.
[52] N. Yousefi, M.M. Gudarzi, Q. Zheng, S.H. Aboutalebi, F. Sharif, J.K. Kim, Self-alignment and high electrical conductivity of ultralarge graphene oxide-polyurethane nanocomposites, J. Mater. Chem. 22 (2012) 12709–12717, https://doi.org/10.1039/c2jm30590a.
[53] V. Kupka, L. Vojtova, Z. Fohlerova, J. Jancar, Solvent free synthesis and structural evaluation of polyurethane films based on poly(Ethylene glycol) and poly (caprolactone), Express Polym. Lett. 10 (6) (2016) 479–492, https://doi.org/10.3144/expresspolymlett.2016.46.
[54] H. Yeganeh, M.M. Lakouraj, S. Jamshidi, Synthesis and properties of biodegradable elastomeric epoxy modified polyurethanes based on poly(ε-caprolactone) and poly (ethylene glycol), Eur. Polym. J. 41 (10) (2005) 2370–2379, https://doi.org/10.1016/j.eurpolymj.2005.05.004.
[55] M. Bendszus, C. Wessig, L. Solymosi, K. Reiners, M. Koltzenburg, MRI of peripheral nerve degeneration and regeneration: correlation with electrophysiology and histology, Exp. Neurol. 188 (2004) 171–177, https://doi.org/10.1016/j.expneurol.2004.03.025.
[56] Z. Ma, Y.i. Hong, D.M. Nelson, J.E. Pichamuthu, C.E. Leeson, W.R. Wagner, Biodegradable polyurethane ureas with variable polyester or polycarbonate soft segments: Effects of crystallinity, molecular weight, and composition on mechanical properties, Biomacromolecules. 12 (9) (2011) 3265–3274, https://doi.org/10.1021/bm2007218.